

XMM-Newton Observations of G32.45 + 0.1 and G38.55 + 0.0: Diffuse Hard X-Ray Sources Found by the ASCA Galactic Plane Survey

Hiroya YAMAGUCHI, Masaru UENO, and Katsuji KOYAMA

Department of Physics, Graduate School of Science, Kyoto University, Sakyo-ku, Kyoto 606-8502
hiroya@cr.scphys.kyoto-u.ac.jp

Aya BAMBA

RIKEN (The Institute of Physical and Chemical Research), 2-1 Hirosawa, Wako, Saitama 351-0198
and

Shigeo YAMAUCHI

Faculty of Humanities and Social Sciences, Iwate University, 3-18-34 Ueda, Morioka, Iwate 020-8550

(Received 2004 April 5; accepted 2004 September 21)

Abstract

We report on XMM-Newton observations of G32.45+0.1 and G38.55+0.0. These were discovered as diffuse hard X-ray sources by the ASCA Galactic Plane Survey, but the limited spatial resolution of ASCA could not conclude whether these are truly diffuse or a group of unresolved point-sources. XMM-Newton, with higher spatial resolution than ASCA, confirmed that G32.45+0.1 has a diffuse shell-like structure with a radius of $\sim 4'$. The spectrum shows a featureless continuum, and can thus be fitted by a power-law model of $\Gamma \sim 2.2$ with an absorption of $N_{\text{H}} \sim 5.2 \times 10^{22} \text{ cm}^{-2}$. From this N_{H} value, we estimated the distance to G32.45+0.1 to be ~ 17 kpc. Thus, the luminosity (in the 0.5–10.0 keV band) and radius of the shell are $\sim 9.5 \times 10^{34} \text{ ergs s}^{-1}$ and ~ 20 pc, respectively. The radio complex sources in the NRAO/VLA Sky Survey (NVSS; 1.4 GHz) are globally associated with the X-ray shell of G32.45+0.1. Therefore, G32.45+0.1 is likely to be a synchrotron-dominant shell-like SNR. No significant diffuse structure was found in the XMM-Newton image of another ASCA diffuse source, G38.55+0.0. The upper limit of the observed flux (0.5–10.0 keV) is estimated to be $9.0 \times 10^{-13} \text{ ergs cm}^{-2} \text{ s}^{-1}$, which is consistent with the ASCA result.

Key words: ISM: individual (G32.45+0.1, G38.55+0.0) — ISM: supernova remnants — X-rays: spectra

1. Introduction

Since cosmic rays were discovered by Hess in 1912, the source and the mechanism of acceleration have been unknown. The spectrum of cosmic rays shows a single power law up to the knee energy ($\sim 10^{15.5}$ eV), where the gyro radius of electrons in the typical interstellar magnetic field is much smaller than the galactic radius. Therefore, cosmic rays below the knee energy are likely to be of galactic origin. The discoveries of synchrotron X-rays and inverse Compton TeV γ -rays from the supernova remnant (SNR) SN 1006 have indicated that electrons are accelerated close to the knee energy (Koyama et al. 1995; Tanimori et al. 1998). The Chandra results of the small-scale structure have been successfully explained by a diffusive shock acceleration model (DSA); the first-order Fermi mechanism is working at the shock front of SNRs (Bamba et al. 2003b; Yamazaki et al. 2004).

Besides SN 1006, synchrotron X-ray emissions were discovered from other SNRs: G347.5–0.3 (RX J1713.7–3946; Koyama et al. 1997; Slane et al. 1997), Cas A (Vink et al. 2000), Tycho's SNR (Hwang et al. 2002), RX J0852.0–4622 (Slane et al. 2001), RCW 86 (Borkowski et al. 2001a), AX J1843.8–0352 (Bamba et al. 2001; Ueno et al. 2003), 30 Dor C (Bamba et al. 2004). Although synchrotron X-ray emissions were observed from several SNRs, the total number and the X-ray fluxes so far discovered are insufficient to account for all of the cosmic rays in our Galaxy; if SNRs are

the main accelerator of the cosmic rays, we can expect more non-thermal SNRs. Accordingly, we searched for SNR candidates in the data of the ASCA Galactic Plane Survey, which covered $|l| \leq 45^\circ$, $|b| \leq 0.4^\circ$ on the galactic plane (Yamauchi et al. 2002). About half a dozen candidates were found in this survey area; follow-up deep exposure observations with ASCA were made on three candidates: G11.0+0.0, G25.5+0.0, and G26.6–0.1, which were suggested to be non-thermal SNRs (Bamba et al. 2003a). G28.6–0.1 (AX J1843.8–0352) was deeply observed with both ASCA and Chandra, and established to be a synchrotron X-ray emitting shell-like SNR (Bamba et al. 2001; Ueno et al. 2003).

Two other candidates, G32.45+0.1 and G38.55+0.0, are seen as diffuse-like hard sources in the ASCA images, and the spectra show a power-law like feature with $\Gamma \sim 1$ –3. The spatial sizes (\sim a few arcmin), however, are marginally compared with the ASCA point spread function (PSF) of (~ 1 arcmin) to determine whether these are diffuse or a group of unresolved point-sources. We, therefore, made XMM-Newton (Aschenbach et al. 2000) observations on G32.45+0.1 and G38.55+0.0 with higher spatial resolution (PSF ~ 5 arcsec) and a larger effective area than those of ASCA.

2. Observations

G32.45+0.1 and G38.55+0.0 were observed with XMM-Newton on 2003 September 25 (Observation ID=0136030101)

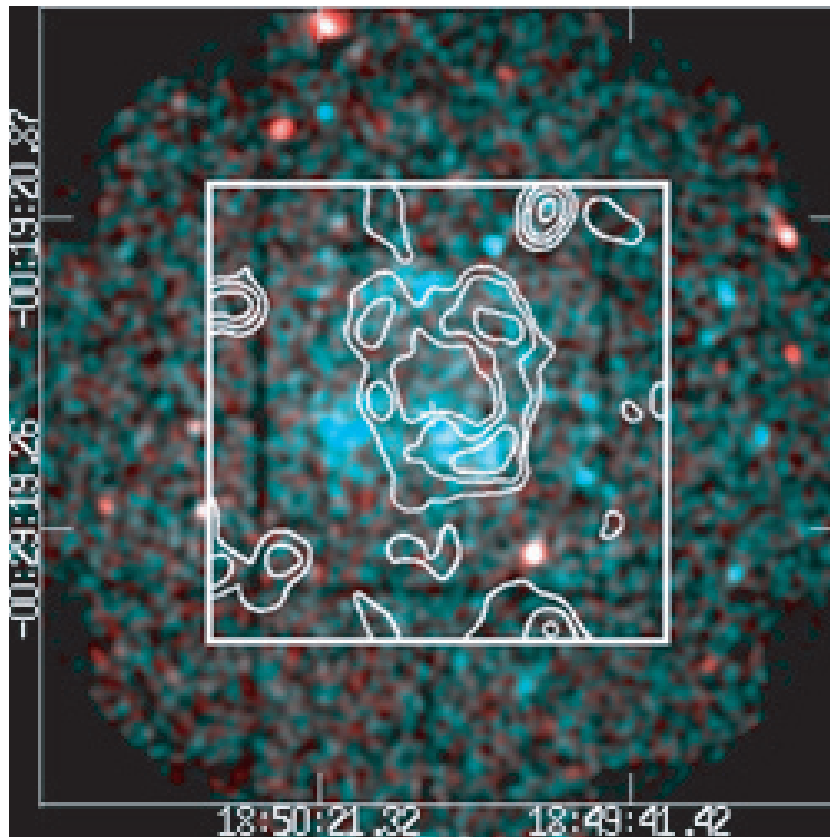


Fig. 1. XMM-Newton/MOS1+2 image of G32.45+0.1 overlaid on the NVSS 20 cm radio contours, which are expressed on the inner region of the square (Condon et al. 1998). The soft (0.5–2.0 keV) band and hard (2.0–7.0 keV) band images are represented by red and blue colors, where the background events are not subtracted. The image has been smoothed to a resolution of $9''.6$. The coordinates (R.A. and Dec.) are referred to J2000.

and 2003 September 21 (Observation ID = 0136030201), respectively. Although the data were obtained from both the EPIC-MOS (Turner et al. 2001) and EPIC-PN (Strüder et al. 2001) cameras, major parts of these objects were suffered by the PN-CCD gaps and bad columns, and we verified that cleaned PN data did not improve the accuracy of the results obtained with only MOS. We thus ignore the PN data hereafter. All of the EPIC instruments were operated in the full-frame mode with a medium filter. We used version 5.4.1 of the Standard Analysis System (SAS) software, and selected X-ray events with PATTERN keywords between 0 and 12.

The net exposure times were 26.8 ks and 15.9 ks for G32.45+0.1 and G38.55+0.0, respectively. In the observation of G32.45+0.1, however, the particle background was exceptionally high and variable, and hence we accumulated a background light-curve in the 10–12 keV band from the whole field of view, and removed the high-background data (the time intervals when the count rate was larger than $0.3 \text{ counts s}^{-1}$). After filtering, the exposure times of MOS1 and MOS2 were 20.5 ks and 21.2 ks, respectively. Filtering using the same prescription was also performed on the observation of G38.55+0.0. The filtered exposure times of MOS1 and MOS2 became 15.1 ks and 15.4 ks, respectively.

In order to estimate the residual soft-proton contamination (which is vignettted), we calculated the “R” value according to

section B.2 of De Luca and Molendi (2004). For both of observations, the R values of MOS1 and MOS2 were 1.2 and 1.1, respectively, and hence contributions of residual soft-protons were negligible in the filtered data.

3. Analysis of G32.45+0.1

3.1. X-Ray Image

In figure 1, the soft (0.5–2.0 keV) and hard (2.0–7.0 keV) band X-ray images are shown with two colors. In the hard-band image (blue) only, we can see a shell-like structure with a radius of about $4'$.

In order to estimate the accurate flux of the diffuse shell in the hard-band image, we picked up point-sources using the EWAVELET software, with a detection threshold of 5σ . Thus detected point-sources are indicated by the black and (thin) white circles in figure 2. The three white circles are in the diffuse shell, and hence we made radial profiles of these sources, and estimated the FWHM assuming a Gaussian profile. As listed in table 1, all of the FWHMs of the sources are significantly larger than that of the point spread function (PSF) of XMM-Newton (FWHM $\sim 5''$). We, therefore, conclude that these are not point-like sources, but are local enhancements on the shell.

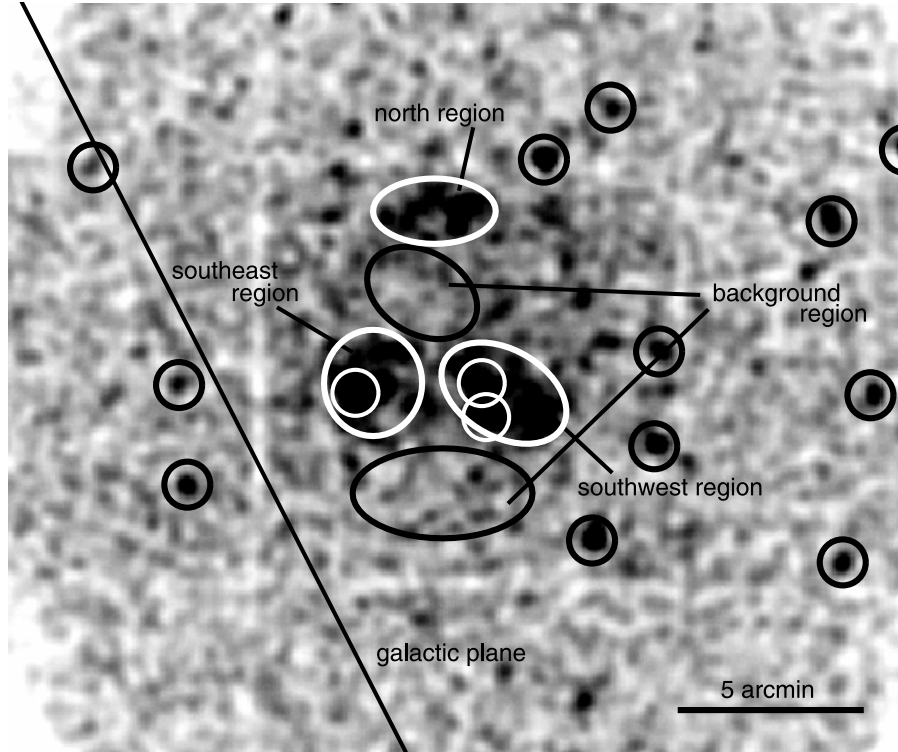


Fig. 2. XMM-Newton/MOS1+2 hard-band image in the 2–7 keV band. The background events were not subtracted. The solid line means the galactic plane. The three (bold) white ellipses and the two black ellipses are source and background regions, respectively. Point-sources are expressed as the black small circles.

Table 1. The position and the extension of the point-like sources in the shell (white circles in figure 2).

(R.A., Dec.) _{J2000}	Position	Extension (FWHM arcsec)
(18 ^h 50 ^m 19 ^s , –00°26′20″)	the southeast region	60 ± 25
(18 ^h 50 ^m 06 ^s , –00°25′58″)	the southwest region	60 ± 25
(18 ^h 50 ^m 05 ^s , –00°26′58″)	the southwest region	26 ± 6.1

Uncertainties correspond to 1 σ regions.

3.2. Spectrum

Firstly, we divided the diffuse emission into three regions (north, southwest, and southeast; figure 2), and extracted the X-ray spectra separately. However the statistics of all the spectra are not sufficient for spectral fittings. We therefore added them together and regarded the result as the spectrum of the whole shell. The background was taken from the neighborhood ellipses, which are also shown in figure 2. Since these background regions are sufficiently near to the source regions, and their average off-axis angle is almost equal to that of the source regions, the contribution of the vignetting effect was negligible in these spectral measurements, and hence we did not apply any vignetting correction. The background-subtracted spectra of MOS1 and MOS2 are shown in figure 3. Since the spectra have no emission line, we fitted them with a model of a power law modified by photo-electric absorption. The cross-sections were taken from Morrison and McCammon (1983). The fittings were statistically accepted for the spectra

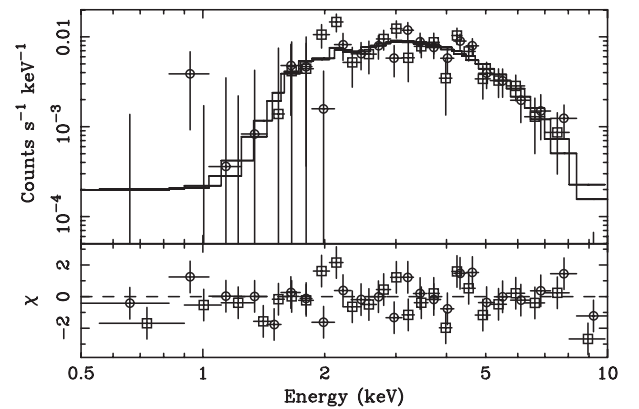


Fig. 3. X-ray spectra of G32.45+0.1 observed with MOS1 (circle) and MOS2 (square). The solid lines show the best-fit power-law models.

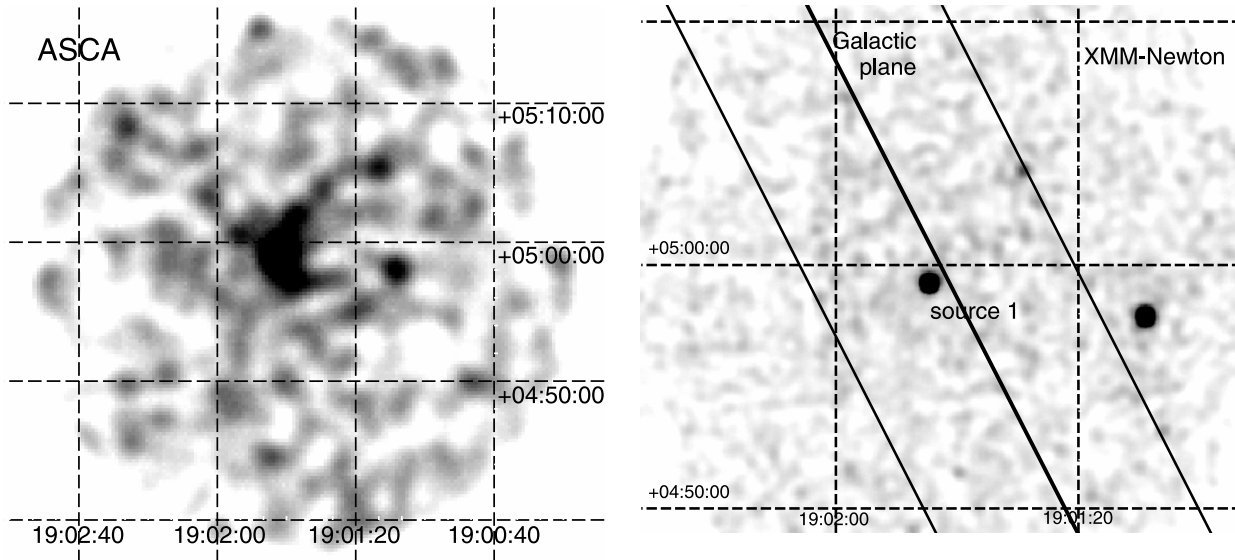


Fig. 4. ASCA/GIS2+3 and XMM-Newton/MOS1+2 images of the G38.55+0.0 region in the hard X-ray band where the background events were not subtracted. The axis labels represent the R.A. and Dec. (J2000) coordinates. The center line and the two outer lines drawn in the right panel mean the galactic plane and $b = \pm 5'$, respectively.

with the best-fit parameters, shown in table 2.

For comparison, we tried fittings with a thin thermal plasma model in non-equilibrium ionization (an NEI model; Borkowski et al. 2001b), and obtained a nearly equal fit. The best-fit parameters of the NEI model are given in table 2.

4. Analysis of G38.55 + 0.0

The EPIC/MOS1+2 image in the 2.0–7.0 keV band near G38.55+0.0 is shown in the right panel of figure 4. For comparison, we show the ASCA image in the same energy band (2.0–7.0 keV band) near the G38.55+0.0 region in the left panel of figure 4. Although we can see a structure extending more than the point spread function (PSF) of ASCA ($\sim 1'$), no significant diffuse emission, except for some point-sources, is found in the XMM-Newton image. The possibility of a group of unresolved point-sources may be excluded, because only one point-source is found near the center of G38.55+0.0 by the XMM-Newton observation of PSF $\sim 5''$ (FWHM).

We first extracted the spectrum of the point-source (source 1) at the center of G38.55+0.0. The source region was selected from a $25''$ -radius circle, and the background was taken from an annular region around the source with inner and outer radii of $25''$ and $100''$. We fitted the background-subtracted spectrum with a power-law model. The fitting was statistically accepted with the best-fit parameters given in table 3. For comparison, we obtained the ASCA spectrum from a $6'$ -radius region with the background from an annulus having an inner-outer radius of $6'$ – $12'$. The background-subtracted spectrum was also fitted with a power-law model. The best-fit parameters are given in table 3. Within the statistical error, we can see no significant difference in the best-fit N_{H} and Γ for the ASCA “diffuse” emission and the XMM-Newton point-source emission. However, the observed flux of ASCA is ~ 5 -times larger than that of source 1 in the XMM-Newton image. Therefore, one possibility is that there is a “diffuse” component with a low surface brightness.

In order to estimate the flux of the putative “diffuse”

Table 2. Results of a spectral fitting of G32.45+0.1.*

Parameters	Power-law	NEI
$N_{\text{H}} [\times 10^{22} \text{cm}^{-2}]$	5.2 (3.9–7.5)	4.6 (3.4–6.1)
Γ/kT [keV]	2.2 (1.8–3.0)	5.2 (3.0–12)
Abundance [†]	...	1.0×10^{-2} (< 0.35)
$n_e t$ [$\text{cm}^{-3} \text{s}$]	...	$3.7 \times 10^{13\ddagger}$
Flux [§] [$\text{ergs cm}^{-2} \text{s}^{-1}$]	2.8×10^{-12}	1.9×10^{-12}
Reduced χ^2 (d.o.f.)	1.14 (46)	1.19 (44)

* Parentheses indicate single-parameter 90% confidence intervals.

[†] Assuming the solar abundance ratio (Anders, Grevesse 1989).

[‡] The error could not be determined in the region of $(1 \times 10^8 - 5 \times 10^{13})$, which is the limit of XSPEC software.

[§] Absorption-corrected flux in the 0.5–10.0 keV band.

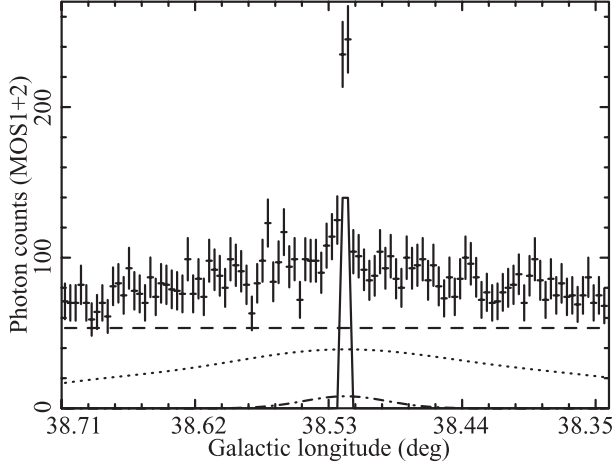


Fig. 5. The projected profile of the sum of the MOS1 and MOS2 photon counts in the 2–7 keV band in the $|b| \leq 5'$ region along l (galactic longitude). The solid, dash, dotted, and dash-dotted lines show the best-fit curves of point-source 1, NXB, CXB+GRXE, and the putative “diffuse” emission, respectively.

emission in the XMM-Newton observation, we made a projected profile along the galactic plane with a width of $|b| \leq 5'$ using the hard-band image (2–7 keV; see figure 4). The profile was then fitted with a model function made under the following assumptions: the non-X-ray background (NXB) is constant in the XMM-Newton-field of view, the cosmic X-ray background (CXB) and the galactic ridge emission (GRXE) are also constant along the galactic plane, but are modified by a vignetting effect, and the contribution of source 1 is given by a Gaussian profile with the width of PSF. In addition, we approximated the putative “diffuse” emission to be a simple Gaussian of $3\sigma = 5'$ with the center at the source 1 position (see the ASCA image). Figure 5 is the projected profile and the best-fit model; NXB is shown by the dash line, the sum of CXB and GRXE is given by the dotted line, and source 1 is shown by the solid line. With this fitting, the flux of the putative “diffuse” emission is constrained to be less than $0.018 \text{ counts s}^{-1}$ (90% upper limit). Thus, this component is undetected in the XMM-Newton observation, unlike the ASCA observation. A reason for this may be a higher particle background than that of the ASCA observation.

This value was converted to $6.4 \times 10^{-13} \text{ ergs cm}^{-2} \text{ s}^{-1}$ (in 0.5–10 keV) under the power-law model with $\Gamma = 1.1$

and $N_{\text{H}} = 2.0 \times 10^{22} \text{ cm}^{-2}$ (the best-fit ASCA parameters of G38.55+0.0).

5. Discussion

5.1. G32.45+0.1

We found a clear shell structure with a radius of $\sim 4'$ in the XMM-Newton hard-band (2.0–7.0 keV) image. The X-ray spectrum was well-fitted with either a power-law or a thin thermal plasma model. The thermal model requires a temperature of 3.0–12 keV, which is similar to (or higher than) that of typical young SNRs, such as Cas A and Tycho’s SNR [$kT \sim 2$ –4 keV; e.g., Vink et al. 1996, Gotthelf et al. 2001 (Cas A); Fink et al. 1994 (Tycho’s SNR)]. This model, however, also requires an uncomfortably low metal abundance (< 0.35 solar abundance), compared with Cas A and Tycho’s SNR (~ 2 solar abundance). Thus, the spectrum of G32.45+0.1 is likely to be a power law. The best-fit parameter of $N_{\text{H}} = 5.2(3.9\text{--}7.5) \times 10^{22} \text{ cm}^{-2}$ gives a rough estimation of the source distance to be 17 kpc with an assumption that the density in the galactic plane is 1 H cm^{-3} . Thus, the X-ray luminosity (0.5–10.0 keV) and the radius are estimated to be $\sim 9.5 \times 10^{34} \text{ ergs s}^{-1}$ and $\sim 20 \text{ pc}$, respectively. These values are not very different from those of the non-thermal component of SN 1006 ($\sim 2.0 \times 10^{34} \text{ ergs s}^{-1}$ and $\sim 9.5 \text{ pc}$; e.g., Dyer et al. 2004).

We found a radio shell at the position of G32.45+0.1 from the NRAO/VLA Sky Survey (NVSS) data at 1.4 GHz (Condon et al. 1998), over-plotted with contours in figure 1, although the authors regarded the radio shell as 7 individual (point-like) sources, as listed in the NVSS catalogue. The flux sum is $\sim 1.7 \times 10^{-1} \text{ Jy}$. From the shell-like morphology in both the radio and X-ray bands and the X-ray power-law model of a photon index of $\Gamma = 2.2(1.8\text{--}3.0)$, G32.45+0.1 is highly possible to be a synchrotron X-ray emitting shell-type SNR. For discussing a wide band spectrum, we fitted the X-ray spectrum with an SRCUT model (Reynolds, Keohane 1999). The radio index has not yet been determined, but a simple acceleration model predicts the energy index to be 0.5. In fact, the energy index (α) at 1 GHz of SN 1006, the typical synchrotron X-ray SNR, is reported to be ~ 0.57 (Allen et al. 2001). We thus tried fitting while assuming α to be 0.5 or 0.6. The best-fit parameters are given in table 5.

Here, the absorption is consistent with the fitting result with the power-law model. Using the values of the cut-off frequency, we can estimate the maximum energy of electrons accelerated by the SNR shock according to Reynolds and

Table 3. Results of spectral fittings of source 1 and the ASCA “diffuse” emission.*

Parameter	Source 1 (XMM-Newton)	ASCA $6'$ -radius region
$N_{\text{H}}[\times 10^{22} \text{ cm}^{-2}]$	3.3 (2.0–5.3)	2.0 (1.6–2.6)
Γ	1.7 (1.1–2.7)	1.1 (0.9–1.3)
Observed flux [†] [$\text{ergs cm}^{-2} \text{ s}^{-1}$]	$2.6 (2.4\text{--}2.9) \times 10^{-13}$	$1.2 (0.82\text{--}1.6) \times 10^{-12}$
N_{H} corrected flux [†] [$\text{ergs cm}^{-2} \text{ s}^{-1}$]	$5.1 (4.6\text{--}5.7) \times 10^{-13}$	$1.6 (1.1\text{--}2.1) \times 10^{-12}$
Reduced χ^2 (d.o.f.)	0.295 (5)	0.912 (19)

* Parentheses indicate 90% confidence intervals.

[†] Flux in the 0.5–10.0 keV band.

Table 4. Results of the projected profile fitting and flux estimation of the G38.55 + 0.0 region.*

Component	Count rate [†]	Model
NXB [counts s ⁻¹ deg ⁻²]	2.8 (1.8–4.0)	constant
CXB + GRXE [counts s ⁻¹ deg ⁻²]	2.3 (0.43–4.3)	constant [‡]
point-source [counts s ⁻¹]	1.0 (0.68–1.3) × 10 ⁻²	Gaussian
diffuse [counts s ⁻¹]	< 0.018	Gaussian

* Parentheses indicate 90% confidence intervals.

[†] All count rates are the photon rates in the 2–7 keV band.[‡] Constant along the galactic plane, but modified by the vignetting effect.**Table 5.** Best-fit parameters by the SRCUT model.*

Parameters	$\alpha = 0.5^{\dagger}$	$\alpha = 0.6^{\dagger}$
N_{H} [$\times 10^{22}$ cm ⁻²]	5.2 (4.5–6.2)	5.2 (4.4–6.1)
Cut-off frequency [$\times 10^{17}$ Hz]	3.4 (0.79–91)	5.4 (< 35)
Norm [‡]	0.019 (0.017–0.022)	0.11 (0.095–0.12)
Reduced χ^2 (d.o.f.)	1.14 (46)	1.14 (46)

* Parentheses indicate 90% confidence intervals.

[†] Fixed value of α .[‡] Flux density at 1 GHz [Jy].

Keohane (1999). Assuming that the cut-off frequency is 5×10^{17} Hz, the maximum electron energy (E_{max}) is estimated to be

$$E_{\text{max}} \sim 60 \left(\frac{10 \mu\text{G}}{B} \right)^{1/2} \text{ TeV}, \quad (1)$$

where B is the magnetic field in which the electrons are accelerated. This result is consistent with the standard picture of the non-thermal SNRs. For example, E_{max} and B of SN 1006 are 20–70 TeV and 3.5–85 μG , respectively (Bamba et al. 2003b).

In either $\alpha = 0.5$ or 0.6 , the predicted flux density at 1.4 GHz is smaller than the NVSS result. This apparent inconsistency may be attributable to a non-uniform shell structure. In fact, the radio-brightest region shows no X-ray shell (see figure 1). This can be interpreted as meaning that the X-ray emission is dominated in a relatively low B region, because the synchrotron-energy loss rate is proportional to B^2 , and hence the energy loss at the X-ray emitting electron energy may be negligible. The radio shell, on the other hand, may come from a higher B region, where the energy loss of high-energy electrons is significant, and hence X-ray emission is weak. A more quantitative study requires spatially resolved X-ray and radio spectroscopy, which is beyond the scope of this paper.

5.2. G38.55 + 0.0

In contrast to the ASCA results, no significant diffuse emission was detected in the XMM-Newton image of the G38.55 + 0.0 region. The absorbed surface brightness (2.0–10.0 keV) of the GRXE is $\sim 3.5 \times 10^{-11}$ ergs cm⁻² s⁻¹ deg⁻² at $l = 38^{\circ}55$ (Sugizaki et al. 2001). Assuming a thin thermal plasma of 7 keV for GRXE (Kaneda et al. 1997), the XMM-Newton count is estimated to be ~ 1.0 counts s⁻¹ deg⁻². The unabsorbed surface brightness of

the CXB component (in 2.0–10.0 keV), on the other hand, is $\sim 1.8 \times 10^{-11}$ ergs cm⁻² s⁻¹ deg⁻² (Ishisaki 1996). With a galactic absorption of $N_{\text{H}} = 3.0 \times 10^{22}$ cm⁻², the count rate is estimated to be ~ 1.0 counts s⁻¹ deg⁻². Thus, the sum (GRXE + CXB) is ~ 2.0 counts s⁻¹ deg⁻². This value is consistent with the best-fit result of the projected profile in table 4 (2.3 counts s⁻¹ deg⁻²). Thus, our flux estimation based on the model fitting to the projected profile is reliable. We then obtained the absorbed flux upper limit of the putative “diffuse” emission to be 6.4×10^{-13} ergs cm⁻² s⁻¹ (0.5–10 keV band), and the absorbed flux of the resolved point-source to be 2.6×10^{-13} ergs cm⁻² s⁻¹ in the same energy band. Thus, the sum of these fluxes is 9.0×10^{-13} ergs cm⁻² s⁻¹, which is consistent with the ASCA observed flux of G38.55 + 0.0. We note that no radio counterpart at the position of G38.55 + 0.0 has been reported. Accordingly, whether G38.55 + 0.0 is a diffuse source or a new SNR is still an open question.

6. Summary

The results of XMM-Newton observations and analyses of G32.45 + 0.1 and G38.55 + 0.0 are summarized as follows:

1. G32.45 + 0.1 shows a clear shell-like structure in the hard X-ray band.
2. The spectrum of G32.45 + 0.1 shows a non-thermal feature, and can be fitted with a power-law model of $\Gamma \sim 2.2$, which suggests synchrotron X-ray emission from the shell of the SNR.
3. The N_{H} value of $\sim 5.2 \times 10^{22}$ cm⁻² gives the source distance to be 17 kpc. Thus, the X-ray luminosity in the 0.5–10.0 keV band and the shell radius of G32.45 + 0.1 are estimated to be $\sim 9.5 \times 10^{34}$ ergs s⁻¹ and 20 pc, respectively.

4. No significant diffuse emission from G38.55+0.0 was detected. The upper limit in the 0.5–10.0 keV band is $\sim 9.0 \times 10^{-13}$ ergs cm $^{-2}$ s $^{-1}$, consistent with the ASCA flux.

We thank all of the members of the ASCA galactic plane survey team. M.U. is supported by JSPS Research Fellowship for Young Scientists. This work is supported by a Grant-in-Aid for the 21st century COE, “Center for Diversity and Universality in Physics”.

References

- Allen, G. E., Petre, R., & Gotthelf, E. V. 2001, *ApJ*, 558, 739
- Anders, E., & Grevesse, N. 1989, *Geochim. Cosmochim. Acta*, 53, 197
- Aschenbach, B., Briel, U. G., Haberl, F., Braeuninger, H. W., Burkert, W., Oppitz, A., Gondoin, P., & Lumb, D. H. 2000, *Proc. SPIE*, 4012, 731
- Bamba, A., Ueno, M., Koyama, K., & Yamauchi, S. 2001, *PASJ*, 53, L21
- Bamba, A., Ueno, M., Koyama, K., & Yamauchi, S. 2003a, *ApJ*, 589, 253
- Bamba, A., Ueno, M., Nakajima, H., & Koyama, K. 2004, *ApJ*, 602, 257
- Bamba, A., Yamazaki, R., Ueno, M., & Koyama, K. 2003b, *ApJ*, 589, 827
- Borkowski, K. J., Lyerly, W. J., & Reynolds, S. P. 2001b, *ApJ*, 548, 820
- Borkowski, K. J., Rho, J., Reynolds, S. P., & Dyer, K. K. 2001a, *ApJ*, 550, 334
- Condon, J. J., Cotton, W. D., Greisen, E. W., Yin, Q. F., Perley, R. A., Taylor, G. B., & Broderick, J. J. 1998, *AJ*, 115, 1693
- De Luca, A., & Molendi, S. 2004, *A&A*, 419, 837
- Dyer, K. K., Reynolds, S. P., & Borkowski, K. J. 2004, *ApJ*, 600, 752
- Fink, H. H., Asaoka, I., Brinkmann, W., Kawai, N., & Koyama, K. 1994, *A&A*, 283, 635
- Gotthelf, E. V., Koralesky, B., Rudnick, L., Jones, T. W., Hwang, U., & Petre, R. 2001, *ApJ*, 552, L39
- Hwang, U., Decourchelle, A., Holt, S. S., & Petre, R. 2002, *ApJ*, 581, 1101
- Ishisaki, Y. 1996, PhD Thesis, The University of Tokyo
- Kaneda, H., Makishima, K., Yamauchi, S., Koyama, K., Matsuzaki, K., & Yamasaki, N. Y. 1997, *ApJ*, 491, 638
- Koyama, K., Kinugasa, K., Matsuzaki, K., Nishiuchi, M., Sugizaki, M., Torii, K., Yamauchi, S., & Aschenbach, B. 1997, *PASJ*, 49, L7
- Koyama, K., Petre, R., Gotthelf, E. V., Hwang, U., Matsuura, M., Ozaki, M., & Holt, S. S. 1995, *Nature*, 378, 255
- Morrison, R., & McCammon, D. 1983, *ApJ*, 270, 119
- Reynolds, S. P., & Keohane, J. W. 1999, *ApJ*, 525, 368
- Slane, P., Hughes, J. P., Edgar, R. J., Plucinsky, P. P., Miyata, E., Tsunemi, H., & Aschenbach, B. 2001, *ApJ*, 548, 814
- Slane, P., Plucinsky, P., Harrus, I. M., Hughes, J. P., Green, A. J., & Gaensler, B. M. 1997, *BAAS*, 29, 1368
- Strüder, L., et al. 2001, *A&A*, 365, L18
- Sugizaki, M., Mitsuda, K., Kaneda, H., Matsuzaki, K., Yamauchi, S., & Koyama, K. 2001, *ApJS*, 134, 77
- Tanimori, T., et al. 1998, *ApJ*, 497, L25
- Turner, M. J. L., et al. 2001, *A&A*, 365, L27
- Ueno, M., Bamba, A., Koyama, K., & Ebisawa, K. 2003, *ApJ*, 588, 338
- Vink, J., Kaastra, J. S., & Bleeker, J. A. M. 1996, *A&A*, 307, L41
- Vink, J., Kaastra, J. S., Bleeker, J. A. M., & Bloemen, H. 2000, *Adv. Space Res.*, 25, 689
- Yamauchi, S., et al. 2002, *IAU 8th Asian-Pacific Regional Meeting*, vol. II, 81
- Yamazaki, R., Yoshida, T., Terasawa, T., Bamba, A., & Koyama, K. 2004, *A&A*, 416, 595

